Phonon spectrum of $ZnAl_2O_4$ spinel from inelastic neutron scattering and first-principles calculations

C. M. Fang,[1] C.-K. Loong,[2] G. A. de Wijs,[3] and G. de With[1]
[1]*Laboratory of Solid State and Materials Chemistry, Eindhoven University of Technology, P.O. Box 513, NL-5600 MB, Eindhoven, The Netherlands*
[2]*Intense Pulsed Neutron Source Division, Argonne National Laboratory, Argonne, Illinois 60439*
[3]*Electronic Structure of Materials, Research Institute for Materials, Faculty of Sciences, Toernooiveld 1, NL-6525 ED, Nijmegen, The Netherlands*

(Received 25 March 2002; revised manuscript received 1 July 2002; published 8 October 2002)

The phonon spectrum of $ZnAl_2O_4$ spinel was investigated jointly by inelastic neutron-scattering and first-principles calculations. The results permit an assessment of important mechanical and thermodynamical properties such as the bulk modulus, elastic constants, lattice specific heat, vibration energy, and Debye temperature. The observed generalized phonon density of states shows a gapless spectrum extending to a cutoff energy of $\sim$840 cm^{-1}. The theoretical results reproduce all of the features of the phonon density of states. The calculated Raman-and infrared-active phonon frequencies agree well with the data in the literature. A comparison of the lattice dynamics of $ZnAl_2O_4$ and $MgAl_2O_4$ spinels was carried out using a simple rigid-ion model, which shows that the major difference in the phonon frequencies of the two materials can be accounted for by the mass effects between the Zn and Mg ions.

DOI: 10.1103/PhysRevB.66.144301 PACS number(s): 71.15.Mb, 61.12.Ex, 62.20.Dc, 65.40.−b

I. INTRODUCTION

Oxide spinels comprise a rich variety of compounds.[1,2] They exhibit many different physical properties and are of great technological and geophysical interest.[2,3] While many oxide spinels, such as $MgAl_2O_4$, show a varying extent of cation disorder,[1,2,4] zinc aluminate spinel $ZnAl_2O_4$ (hereafter referred to as Zn spinel) is one of the exceptions that shows only small departures from the cation distribution of an ideal spinel structure.[5–7] As a natural mineral Zn spinel is called gahnite. It has a combination of robust properties: high melting temperature, high strength, and high resistance to chemical attack.[2,8] As a bulk ceramic, it has been used as a structural and high-temperature material. Synthetic, high-surface-area Zn spinels are useful as catalysts and catalytic supports.[9–12] Furthermore, Zn spinel shows interesting stress-induced luminescence properties.[13,14]

The crystal structure of Zn spinel[1] is isostructural with that of spinel $MgAl_2O_4$ [space group $Fd3m$, No. 227 (Ref. 15)], which was first determined by Bragg[16] and Nishikawa[17] independently. There are 8 f.u. per conventional unit cell, which consists of 32 anions (O ions) and 24 cations (Zn and Al ions). The Bravais lattice of an ideal spinel structure consists of an fcc sublattice of O with the divalent cations (Zn^{2+}) and trivalent cations (Al^{3+}) occupying one-eighth of the interstitial tetrahedral sites and one-half of the octahedral sites, respectively. The crystal structure of spinels is completely defined by the lattice parameter a and the anions' positional parameter x.[1,2] The primitive cell contains 2 f.u., giving rise to a total of 42 phonon branches.

The vibrational properties of Zn spinel were mainly studied with Raman[18] and infrared[18–22] (IR) spectroscopies. We are not aware of any report of inelastic neutron-scattering measurements on Zn spinel in the literature. Thus, experimental data of phonon frequencies are limited to the vicinity of the Γ point of the Brillouin zone (BZ). Chopelas and Hofmeister[18] measured the Raman spectrum of Zn spinel and reported five vibrational frequencies. Infrared studies by various workers, on the other hand, revealed some inconsistency in the data. Hafner[20] and Brunel and Vierne[21] reported three broad peaks at about 667, 562, and 510 cm^{-1} and at about 704, 578, and 512 cm^{-1}, respectively, in the IR absorption and reflection spectra of gahnite. Gadsden[19] combined the experimental data of Hafner[20] and Brunel and Vierne[21] in an analysis and obtained a complex group of IR frequencies at 750, 690, 670, 650, 590, 562, and 510 cm^{-1}. Alvarez, Bosch, and Valenzuela[22] measured the IR spectrum of synthetic Zn spinel samples. They concluded, based on simulations using the classic pair-potential method with rigid ions, that the modes at 505 and 562 cm^{-1} originate from Zn-O vibrations, while the bands observed in the range of 600–1400 cm^{-1} are due to Al-O vibrations.[22] Chopelas and Hofmeister[18] analyzed the IR spectrum of the mineral using the Kramers-Kronig method. They identified four vibrational [transverse optic (longitudinal optic), TO (LO)] frequencies at 220 (231), 486 (533), 543 (608), and 641 (787) cm^{-1}, as well as additional peaks of TO overtones at 754, 838, and 850 cm^{-1}.

In this paper, we report a phonon density-of-states measurement of Zn spinel by means of inelastic neutron-scattering and a first-principles calculation of the phonon-dispersion curves. In principle, neutron spectroscopy is a more complete method for measuring phonon spectra of crystalline solids than optical spectroscopy because neutrons interact with phonons throughout the entire BZ and the technique is not subject to restriction by selection rules.[23] However, as a large single crystal of Zn spinel is unavailable, neutron measurements using polycrystalline samples provide only a measure of the phonon density of states. In this case, the first-principles calculation of the phonon spectrum is important for a full characterization of the phonon spectrum.

TABLE I. Calculated lattice parameters and interatomic distances (Å) for $ZnAl_2O_4$, as compared with the experimental results.

	Theor.	Expt.[a]
Space group	$Fd3m$	
a (Å)	7.998	8.064
x of O atoms	0.389	0.390
Bonding		
Zn-O (4×)	1.93	1.94
Al-O (6×)	1.89	1.90
Mechanical properties		
B (GPa)	218	202[b]
c_{11} (GPa)	316	
c_{12} (GPa)	169	
c_{44} (GPa)	148	

[a]Reference 1.
[b]Reference 39.

The neutron data provide a means to validate and refine the theoretical calculations. As a result, the model unambiguously identifies the frequencies and the atomic motion of the Raman- and IR-active modes. The phonon spectrum of Zn spinel is compared with that of $MgAl_2O_4$ spinel[24] using a simple rigid-ion model for an understanding of the effects on the phonons due to the mass difference between the Mg and Zn ions. The mechanical (elastic constants and modulus) and thermal (specific heat and Debye temperature) properties were also obtained. The results are useful for the analysis of the thermodynamic properties of compounds with the spinel-type structure.

II. EXPERIMENTAL AND THEORETICAL DETAILS

$ZnAl_2O_4$ powders were prepared by a conventional solid-state synthesis method. Powders of ZnO and α-Al_2O_3 were first mixed in a ball mill for 24 h. The mixture was slowly heated to 1400 °C and kept at that temperature for 12 h until Zn spinel was formed completely. X-ray diffraction showed that the sample was a single-phase spinel structure with no detectable impurities.

Neutron-inelastic-scattering experiments were performed using the low-resolution medium-energy Chopper Spectrometer at the Intense Pulsed Neutron Source of the Argonne National Laboratory, IL. The energy resolution (full width at half maximum) varies from ~8% of the incident energy in the elastic region to ~2% near the end of the neutron energy-loss spectrum.[25] Neutrons with incident energies of 200 and 80 meV were used to measure the phonon spectra over the 0–150 meV range with good resolution. The energy units of meV and cm^{-1}, where 1 meV is equivalent to 8.066 cm^{-1}, are used interchangeably in this paper. A polycrystalline ~40 g sample of Zn spinel was placed inside a sealed aluminum container in the shape of a thin slab (dimension 75×100×2 mm^3), which was mounted on the cold plate of a closed-cycle helium refrigerator at a 45° angle with the incident neutron beam. Such geometry minimized multiple scattering effects. All measurements were performed at 8 K so as to minimize multiphonon scattering. Background scattering was removed from the data by subtracting the intensity of an empty-container run. Measurements of elastic incoherent scattering from a vanadium standard provided detector calibration and intensity normalization.

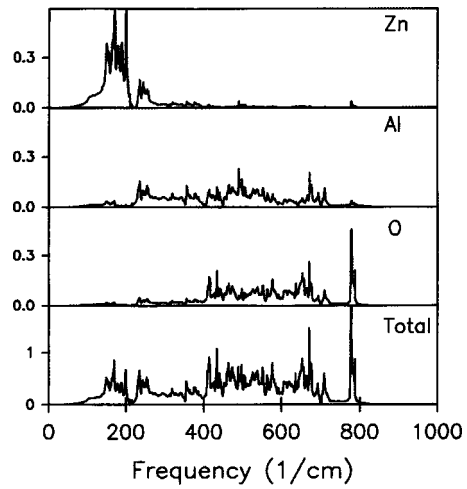

FIG. 1. Partial and total PDOS for Zn spinel calculated from first principles.

The phonon calculations were carried out using the first-principles molecular-dynamics computer code VASP (Vienna *ab initio* simulation program).[26–28] This program first calculates the electronic structure from first principles and then the interatomic forces via the Hellmann-Feynman theorem. The phonon frequencies and eigenvectors were obtained by diagonalization of the dynamical matrix. Details of the methods can be found in Refs. 24 and 29. Calculations were applied to a conventional unit cell (1×1×1), which consists of four primitive unit cells. Periodic boundary conditions were imposed. All internal coordinates of the atoms have been fully relaxed. Selected atoms were displaced slightly (about 0.01–0.05 Å) away from their equilibrium positions, and the corresponding interatomic forces were calculated and then force constants were obtained. Using these force constants, the phonon frequencies were obtained by straightforward di-

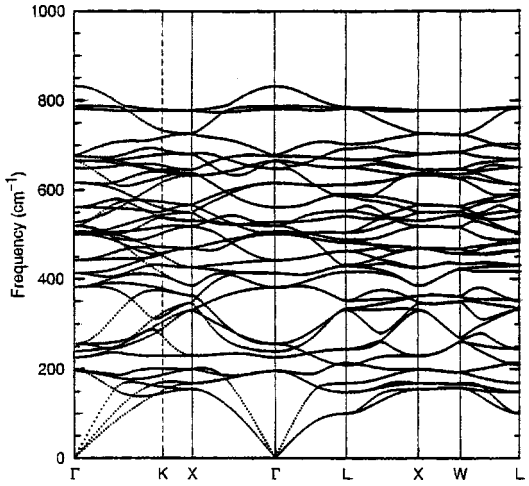

FIG. 2. Calculated phonon-dispersion curves along high-symmetry directions in BZ for Zn spinel.

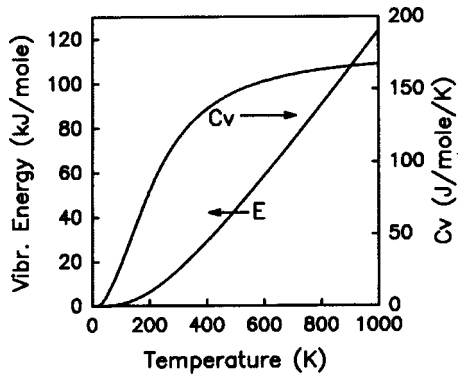

FIG. 3. Vibration energy E and specific heat C_v calculated using the harmonic approximation from the phonon spectrum.

agonalization of the dynamical matrix. This method does not account for the effect of the macroscopic electrostatic field that arises for certain LO modes in the long-wavelength limit ($k \rightarrow \Gamma$). This field lifts the LO-TO degeneracy of the IR-active modes. Following Refs. 30 and 31, we corrected for the effect of the macroscopic field and the calculated frequency shifts of the LO modes. For the determination of the LO frequencies the interplanar force constants were calculated using a $2\times1\times1$ cell (which contains eight primitive cells with a total length of about 16 Å). The size of this cell was shown be to sufficiently large based on our previous calculations for Mg spinel. In the case of Mg spinel we checked the resulting LO-TO splitting with a longer $3\times1\times1$ cell, and found only minor differences.[24] The phonon-dispersion curves were calculated along several high-symmetry directions in the BZ. The phonon density of states (PDOS) was obtained by linear tetrahedron integration of the phonon frequencies over a $10\times10\times10$ k-point mesh. The symmetry representation of the zone-center modes was examined following White and de Angelis.[32] The crystal symmetry implies five Raman-and four IR-active modes. The elastic constants (c_{11}, c_{12}, and c_{44}) for spinel $ZnAl_2O_4$ were calculated from energy changes due to very small strain components (<3% volume of the ideal structure) in the harmonic approximation. The bulk modulus $B=(c_{11}+2c_{12})/3$ was calculated from a fit of the total energy with respect to

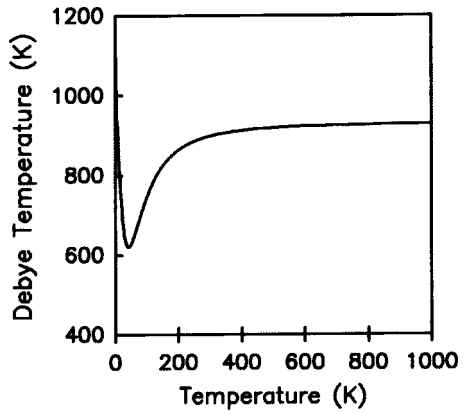

FIG. 4. Debye temperature of Zn spinel calculated from the phonon density of states.

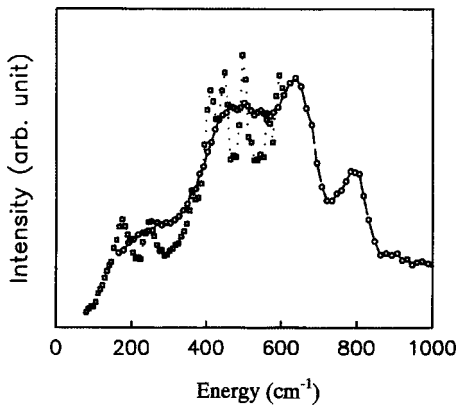

FIG. 5. Measured generalized PDOS for Zn spinel. The circles and squares represent the measured data using neutron incident energies of 200 and 80 meV, respectively.

volume change up to the second order of strain components δ according to Birch and Murnaghan.[33] The elastic constants were obtained from a second-order polynomial fit through the energy distortion curve.

The (bulk) thermal properties (free energy, entropy, and specific heat) of spinel $ZnAl_2O_4$ were obtained from the calculated PDOS within the harmonic approximation according to standard thermodynamics.

The electronic structure calculations were carried out in the local-density approximation (LDA).[34] The electronic wave functions were sampled on a $2\times2\times2$ k-point mesh in the BZ of the conventional unit cell. Additional calculations were carried out for an elongated cell using a consistent k-point mesh. A norm-conserving pseudopotential was used for Al.[35] Ultrasoft pseudopotentials were used for Zn and O.[36,37] The kinetic-energy cutoff on the wave functions was 495 eV (36 Ry). For the (augumentation) charge, a cutoff of 928 eV (68 Ry) was used. These parameters were chosen based on convergence tests for a previous study on

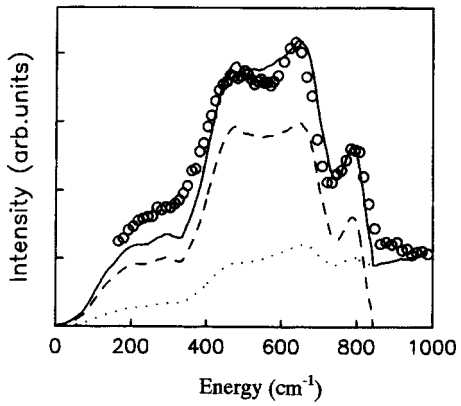

FIG. 6. A comparison of the measured (circles) and calculated (solid line) generalized PDOS of Zn spinel. The experimental data, obtained with a neutron incident energy of 200 meV, contain multiphonon contribution. The calculated spectrum is a sum of the generalized one-phonon DOS (dashed line) and the multiphonon component (dotted line), both of which were convolved with the experimental resolution function.

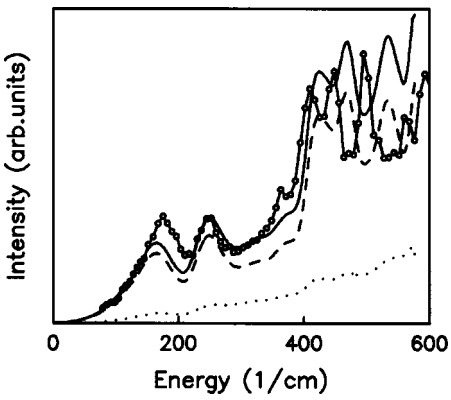

FIG. 7. A comparison of the measured (circles) and calculated (thick solid line) generalized PDOS of Zn spinel. The experimental data were obtained with a neutron incident energy of 80 meV and the line joining the data points is a guide to the eye. The calculated spectrum is a sum of the generalized one-phonon DOS (dashed line) and the multiphonon component (dotted line), both of which were convolved with the experimental resolution function.

$MgAl_2O_4$.[24] Adopting a similar *k*-point mesh for Zn spinel and Mg spinel was justified because of the very similar electronic structure of the two spinels. For Mg spinel the $2\times2\times2$ *k*-point mesh produced essentially the same results as those from a previous study.[24]

III. RESULTS AND DISCUSSIONS

A. Theoretical results

The crystal structure was optimized by a minimization of the total energy, resulting in $a=7.998$ Å and $x=0.389$ for Zn spinel, which compares favorably with the experimental values ($a=8.088$ Å and $x=0.390$).[1] A slight underestimation of the lattice constant is not unusual in LDA calculations. In all subsequent calculations, the optimized calculated values of a and x were used. The lattice parameter of Zn spinel is very close to that of Mg spinel (experimental $a=8.087$ Å) (Refs. 1 and 24) in spite of the fact that the ionic radius of Zn^{2+} (0.74 Å) is larger than that (0.66 Å) of Mg^{2+} ions.[38] The calculated Zn-O distance in Zn spinel is 1.93 Å, the same as the Mg-O distance in Mg spinel. The calculated Al-O distance in Zn spinel (1.89 Å) is slightly smaller than that (1.90 Å) of Mg spinel.

The calculated bulk modulus for Zn spinel is 218 GPa, which is somewhat larger than the experimental value (202 GPa) measured recently by Levy *et al.*[39] It is also slightly larger than the calculated value (207 GPa) for $MgAl_2O_4$ using the same approach.[40] The elastic constants are listed in Table I. From the elastic constants we obtain the anisotropy parameter $A=2c_{44}/(c_{11}-c_{12})=2.02$, which indicates that the elastic properties of Zn spinel are highly anisotropic.

Figure 1 shows the calculated partial and total PDOS for Zn spinel. The total (PDOS) spans up to about 840 cm^{-1}. This result is markedly different from the PDOS obtained using a semiempirical pair-potential method, which shows an energy cutoff as high as 1700 cm^{-1}.[22] The heavy Zn ions are mainly responsible for the low-energy motions (<250 cm^{-1}), whereas the Al and O ions are involved in vibrational modes over a wide range of energies above ~240 cm^{-1}. In particular, O motions are well localized near the end of the phonon spectrum. A sharp peak around 800 cm^{-1} is composed of almost only oxygen vibrations.

TABLE II. Calculated vibration modes at Γ for $ZnAl_2O_4$ as compared with $MgAl_2O_4$.

Species	$ZnAl_2O_4$	$MgAl_2O_4$[a]	$ZnAl_2O_4$[b]
T_{2g} (R)	197	319	211
T_{1u} (IR)	226 (240)	311 (319)	238 (248)
T_{2u}	256	265	265
T_{1g}	382	360	360
E_u	413	412	412
E_g (R)	442	426	426
T_{2u}	501	483	483
T_{1u} (IR)	507 (528)	512 (580)	496 (527)
T_{2g} (R)	520	570	535
T_{1u} (IR)	562 (648)	588 (638)	554 (637)
E_u	615	608	608
T_{2g} (R)	665	682	669
T_{1u} (IR)	675 (832)	698 (866)	693 (849)
A_u	678	668	668
A_u	781	763	763
A_g (R)	784	776	776

[a]Reference 24.

[b]Vibration modes at Γ of $ZnAl_2O_4$ obtained using the force-constant matrix of $MgAl_2O_4$.

The calculated phonon-dispersion curves along the high-symmetry directions are shown in Fig. 2. The 42 phonon branches fill the entire energy range, leaving no gap in the PDOS.

The thermal properties of Zn spinel are obtained from the calculated PDOS. The zero-point vibration energy is 603.83

TABLE III. Comparison between the calculated and experimental Raman and IR spectra.

Modes	Theoretical	Chopelas and Hofmeister[a]	
Raman-active modes			
T_{2g}	197	196	
E_g	442	417	
T_{2g}	520	509	
T_{2g}	665	658	
A_g	785	758	
IR-active modes			
	TO (LO)	TO (LO)[b]	TO[c]
T_{1u}	226 (240)	220(231)	224
	507 (528)	~440(533)	486
	562 (648)	543(608)	551
	675 (832)	641(838)	651

[a]Reference 18.

[b]Experimental data analyzed using the Kramers-Kronig method as per Ref. 18.

[c]TO modes calculated by classic dispersion as per Ref. 18.

meV/f.u. The calculated relationships between the thermal properties (specific heat C_v, vibration energy E, and temperature T) are shown in Fig. 3. The specific heat C_v at room temperature is calculated to be about 116.2 J/K mol.

The Debye model is widely used for ceramic materials. Figure 4 shows the change of the Debye temperature Θ with temperature T for Zn spinel. The Debye temperature changes substantially at the low-temperature range (1–200 K) and reaches a minimum at about 42 K with the Debye temperature 620 K, and then increases with temperature stably. At room temperature the Debye temperature Θ for Zn spinel is about 898 K, which is not far from the value at 1000 K (Θ=928 K).

B. Measured generalized phonon density of states

Inelastic neutron-scattering measurements on a polycrystalline sample over a wide range of detector angles effectively provide an average over all crystallographic orientations. Under these conditions, a generalized PDOS can be obtained from the measured scattering function $S(Q,E)$ according to[41–43]

$$G(E)=\frac{2M}{\hbar^2}\left\langle \frac{e^{-2W(Q)}}{Q^2}\frac{E}{n(E)+1}S(Q,E)\right\rangle \approx M\sum_i \frac{c_i\sigma_i}{M_i}F_i(E), \quad (1)$$

where c_i, σ_i, M_i, and $F_i(E)$ are the concentration, neutron-scattering cross section, mass, and partial PDOS, respectively, for the ith atomic species. M is the mean sample mass, $n(E)$ is the Bose-Einstein distribution function, and $\langle\cdots\rangle$ represents the average over the values of observed wave-vector magnitude Q. The Debye-Waller factors, $e^{-2W(Q)}$, are very close to unity for low-temperature data. It can be seen from Eq. (1) that $G(E)$ provides a measure of the PDOS weighted by the $c_i\sigma_i/M_i$ factors, which is often referred to as the neutron-weighted PDOS. The quantities σ_i/M_i for Zn, Al, and O are 0.0632, 0.0557, and 0.2645 b/g (1 b=1 $\times 10^{-24}$ cm^2). Therefore, the generalized PDOS obtained from a neutron experiment reveals a larger contribution from lattice modes involving the O motion.

Figure 5 shows the generalized PDOS of Zn spinel measured with incident neutron energies of 80 and 200 meV. The 80-meV run reveals more detailed structure because of the better energy resolution. The observed spectrum of the 200-meV run extends beyond 800 cm^{-1} due to contributions from multiple phonon excitations. Using the calculated true partial PDOS, the generalized PDOS is calculated according to Eq. (1) and, as can be seen in Fig. 5, the positions of the salient features agree well with those of the measured generalized PDOS. Therefore, we used the calculated generalized PDOS to estimate the multiphonon contribution, following the Gaussian approximation method described by Sjölander.[44] In Figs. 6 and 7 we compare the resulting generalized PDOS after the removal of the multiphonon component for the 80- and 200-meV runs, respectively, with the calculated generalized PDOS that was convolved with the instrumental resolution functions. The broad phonon bands around 480, 640, and 800 cm^{-1} agree very well with the data of the 200-meV run. In the case of the 80-meV run, the calculated generalized PDOS reproduced the five-band structure at about 175, 248, 410, 448, and 499 cm^{-1} except that the calculated frequencies of the three bands at high energies are somewhat higher than the observed energies. This generally good agreement gives credence to the accuracy of the first-principles calculations.

C. Comparison with optical data

The phonon modes at Γ are classified following White and de Angelis[32] as

$$\Gamma(k=0)=A_{1g}(R)+E_{1g}(R)+3T_{2g}(R)+4T_{1u}(IR)+T_{1g}+2A_{2u}+2E_u+2T_{2u}, \quad (2)$$

where R and IR corresponds to Raman-and infrared-active, respectively. The calculated frequencies of these phonons are listed in Table II.

The experimental Raman frequencies obtained by Chopelas and Hofmeister[18] from mineral samples of gahnite are shown in Table III. In general, the data compare favorably (within 2–4%) with the values from our calculations. The largest difference, which occurred in the E_g mode, is about 6%.

The IR data of Zn spinel are more complex. As summarized by Gadsden[19] the early IR data showed a complex group of values at 750 (shoulder, broad), 690 (shoulder), 670 (strong, broad), 650 (shoulder), 590 (inflection), 562 (strong, broad), and 510 cm^{-1} (strong, broad). Chopelas and Hofmeister[18] analyzed the IR spectrum of the mineral gahnite using the Kramers-Kronig method and found four TO (LO) frequencies, which are compared with the calculated values in Table III. Additionally, extra peaks (TO overtones) were observed at ~846 (850) cm^{-1}. The calculated TO frequencies at 226 and 561 cm^{-1} are in good agreement with the experimental values within 3.3%, while a slightly larger difference of about 5.3% is found for the TO frequency at 675 cm^{-1}. The TO frequency at 507 cm^{-1} is very different from the experimental value of 440 cm^{-1}. The experimental value, however, was assigned based on a broad peak. The calculated LO frequencies are in agreement with the experimental values within 1.0–6.6 %. Our calculated TO frequencies are close (within 5%) to those obtained by Chopelas and Hofmeister.[18]

D. Comparison with Mg spinel

Since Zn spinel is isostructural to Mg spinel and the ionic radius and local bonding environment of Zn and Mg spinel are similar, the major difference in their phonon spectra is expected to arise from the mass difference between Zn and Mg. The phonon frequencies at Γ of Zn spinel are compared with those of Mg spinel in Table II. In order to achieve a better understanding of the mass effect on the vibrational modes at Γ, we performed calculations of the phonon frequencies of Zn spinel using the force constants for Mg spinel but replaced the mass of Mg by that of Zn (a rigid-ion

model). The result is given in Table II. We find that the T_{2g} and T_{1u} modes that contain large contributions from the Zn (or Mg) vibrations are strongly influenced by the mass effect whereas for other species (T_{2u}, T_{1g}, E_u, E_g, A_u, and A_g) the changes are small. In detail, the Raman-active T_{2g} frequencies (211, 535, 669 cm^{-1}) obtained from mass substitution are slightly higher than those (197, 520, 665 cm^{-1}) obtained by the theoretical calculations. All other modes such as the T_{1u} frequencies 238 (248), 496 (527), 554 (637), and 693 (849) cm^{-1} versus 226 (240), 507 (528), 562 (648), and 675 (832) cm^{-1}, respectively (see Table II), show good agreement. Therefore, the lattice dynamics in Zn and Mg spinel are similar and the major change in the phonon frequencies can be accounted for by a rigid-ion model, which only takes the mass effect into account. All other modes such as the T_{2u} frequencies (see Table II) show good agreement.

IV. CONCLUSIONS

Neutron-inelastic-scattering experiments and first-principles calculations have been performed for a parallel study of the phonon spectrum in Zn spinel. The measured generalized PDOS exhibits a gapless spectrum with a cutoff energy at $\sim$840 cm^{-1} and agrees well with the calculations. The calculated partial PDOS indicates that the Zn ions contribute mainly to phonons at low energies (below $\sim$250 cm^{-1}), whereas the Al and O ions partake in lattice vibrations over a wide range of energies (about 240–840 cm^{-1}). The theoretical results identify the Raman and infrared frequencies clearly and, in general, compare well with experimental data. A comparison of the lattice dynamics of Zn and Mg spinel is made using a rigid-ion model that includes only the mass difference between Zn and Mg ions. As a first approximation, this simple model accounts adequately for the major difference in the phonon frequencies, indicating the similarity of the lattice dynamics in these two spinel materials. The calculations also give the mechanical parameters: 218 GPa for the bulk modulus, and 316, 169, and 148 GPa for the elastic constants c_{11}, c_{12}, and c_{44}, respectively. The specific heat and the Debye temperature at 300 K are calculated to about 116.2 J/K mol and 898 K, respectively.

ACKNOWLEDGMENTS

Dr. G. Kresse (University of Vienna) is acknowledged for technical help in the calculations. We thank Professor Ruud Metselaar (SVM, TUE) for helpful discussions and his critical reading of this manuscript. We also thank E. Goremychkin (ANL) for his assistance in the neutron experiment. A portion of this work represents part of the research program of the Stichting voor Fundamenteel Onderzoek der Materie (FOM), and the financial support from the Nederlandse Organisatie voor Wetenschappelijk Onderzoek (NWO) is gratefully acknowledged. Work performed at the Argonne National Laboratory is supported by the U.S. Department of Energy, Basic Energy, Sciences, under Contract No. W-31-109-ENG-38.

[1] N. W. Wyckoff, *Crystal Structures* (Interscience, NY, 1962), Vol. 2.
[2] K. E. Sickafus and R. Hughes, J. Am. Ceram. Soc. **82**, 3277 (1999).
[3] E. G. Ravenstein, Nature (London) **44**, 423 (1891).
[4] N. W. Grimes, Phys. Technol. **6**, 22 (1975).
[5] H. St. C. O'Neill and W. A. Dollase, Phys. Chem. Miner. **20**, 541 (1994).
[6] N. Kashii, H. Maekawa, and Y. Hinatsu, J. Am. Ceram. Soc. **82**, 1844 (1999).
[7] S. Lucchesi, A. Della Giusta, and U. Russo, Miner. Mag. **62**, 41 (1998).
[8] I. Futoshi, G. Naoyuki, and M. Masashi, U.S. Patent No. 5,561,089 (1 October 1996).
[9] J. Wrzyszcz, M. Zawadzki, J. Trawczynski, H. Grabowska, and W. Mista, Appl. Catal., A **210**, 263 (2001).
[10] J. C. J. Bart and R. P. A. Sneeden, Catal. Today **2**, 1 (1987).
[11] M. A. Valenzuela, G. Anguilar, P. Bosch, H. Armendariz, P. Salas, and A. Montoya, Catal. Lett. **15**, 179 (1992).
[12] R. Roesky, J. Weigury, H. Bestgen, and U. Dingerdissen, Appl. Catal., A **176**, 213 (1999).
[13] H. Matsui, C.-N. Xu, and H. Tateyama, Appl. Phys. Lett. **78**, 1068 (2001).
[14] W. Strek, P. Deren, A. Bednarkiewicz, M. Zawadzki, and J. Wryzyszcz, J. Alloys Compd. **300–301**, 456 (2000).
[15] *International Tables for Crystallography*, edited by T. Hahn (Reidel, Dordrecht, 1983), Vol. A.
[16] W. H. Bragg, Philos. Mag. **30**, 305 (1915).
[17] S. Nishikawa, Proc. Tokyo Math.-Phys. Soc. **8**, 199 (1915).
[18] A. Chopelas and A. M. Hofmeister, Phys. Chem. Miner. **18**, 279 (1991).
[19] *Infrared Spectra of Minerals and Related Inorganic Compounds*, edited by J. A. Gadsden (Acford, Chichester, Sussex, 1975).
[20] S. Hafner, Z. Kristallogr. **115**, 331 (1961).
[21] R. Brunel and R. Vierne, Bull. Soc. Fr. Mineral. Cristallogr. **93**, 328 (1970).
[22] L. J. Alvarez, P. Bosch, and M. A. Valenzuela, Catal. Lett. **22**, 361 (1993).
[23] C.-K. Loong, P. Vashishta, P. K. Kaila, W. Jin, M. H. Degani, D. G. Hinks, D. L. Price, J. D. Jorgensen, B. Dabrowski, A. W. Mitchell, D. R. Richards, and Y. Zheng, Phys. Rev. B **45**, 5052 (1992).
[24] G. A. de Wijs, C. M. Fang, G. Kresse, and G. de With, Phys. Rev. B **65**, 094305 (2002).
[25] C.-K. Loong, S. Ikeda, and J. M. Carpenter, Nucl. Instrum. Methods Phys. Res. A **260**, 381 (1987).
[26] G. Kresse and J. Hafner, Phys. Rev. B **47**, 558 (1993); **49**, 14251 (1994).
[27] G. Kresse and J. Furthmueller, Comput. Mater. Sci. **6**, 15 (1996).
[28] G. Kresse and J. Furthmueller, Phys. Rev. B **54**, 11 169 (1996).
[29] G. Kresse, J. Furthmueller, and J. Hafner, Europhys. Lett. **32**, 729 (1995).
[30] G. Kern, G. Kresse, and J. Hafner, Phys. Rev. B **59**, 8551 (1999).

[31] K. Kunc and R. M. Martin, Phys. Rev. Lett. **48**, 406 (1982).
[32] W. B. White and B. A. de Angelis, Spectrochim. Acta, Part A **32**, 985 (1967).
[33] F. D. Murnaghan, Proc. Natl. Acad. Sci. U.S.A. **30**, 244 (1944).
[34] D. M. Ceperley and B. J. Alder, Phys. Rev. Lett. **45**, 566 (1980).
[35] A. M. Appe, K. M. Rabe, E. Kaxiras, and J. D. Joannopoulos, Phys. Rev. B **41**, 1227 (1990).
[36] D. Vanderbilt, Phys. Rev. B **41**, 7892 (1990).
[37] G. Kresse and J. Hafner, J. Phys.: Condens. Matter **6**, 8245 (1994).
[38] *CRC Handbook of Chemistry and Physics*, edited by R. C. Weast (CRC Press, Boca Raton, FL, 1988).
[39] D. Levy, A. Pavese, A. Sani, and V. Pischedda, Phys. Chem. Miner. **28**, 612 (2001).
[40] C. M. Fang and G. de With, Philos. Mag. A (to be published).
[41] D. L. Price and K. Sköld, in *Neutron Scattering*, edited by K. Sköld and D. L. Price, (Academic, Orlando, 1986), Vol. A, p. 29.
[42] V. S. Oskotskii, Fiz. Tverd. Tela (Leningrad) **9**, 550 (1967) [Sov. Phys. Solid State **9**, 420 (1967)].
[43] M. M. Bredov, B. A. Kotov, N. M. Okuneva, V. S. Oskotskii, and A. L. Shakh-Budagov, Fiz. Tverd. Tela (Leningrad) **9**, 287 (1967) [Sov. Phys. Solid State **9**, 214 (1967)].
[44] A. Sjölander, Ark. Fys. **14**, 315 (1958).